Effects of Heat Treatment on the Ballistic Impact Properties of Inconel 718 for Jet Engine Fan Containment Applications

J. Michael Pereira* and Bradley A. Lerch`
National Aeronautics and Space Administration
Glenn Research Center
Cleveland, Ohio 44135

Abstract

The effects of heat treating Inconel 718 on the ballistic impact response and failure mechanisms were studied. Two different annealing conditions and an aged condition were considered. Large differences in the static properties were found between the annealed and the aged material, with the annealed condition having lower strength and hardness and greater elongation than the aged. Correspondingly large differences were found in the velocity required to penetrate material in the two conditions in impact tests involving 12.5 mm diameter, 25.4 mm long cylindrical Ti-6-4 projectiles impacting flat plates at velocities in the range of 150 to 300 m/sec. The annealed material was able to absorb over 25 percent more energy than the aged. This is contrary to results observed for ballistic impact response for higher velocity impacts typically encountered in military applications where it has been shown that there exists a correlation between target hardness and ballistic impact strength. Metallographic examination of impacted plates showed strong indication of failure due to adiabatic shear. In both materials localized bands of large shear deformation were apparent, and microhardness measurements indicated an increase in hardness in these bands compared to the surrounding material. These bands were more localized in the aged material than in the annealed material. In addition the annealed material underwent significantly greater overall deformation before failure. The results indicate that high elongation and better strain hardening capabilities reduce the tendency for shear to localize and result in an unstable adiabatic shear failure. This supports empirical containment design methods that relate containment thickness to the static toughness.

KEYWORDS: Impact; Inconel 718; Containment; Heat treatment

*Corresponding author.

Introduction

International aviation regulatory agencies, such as the Federal Aviation Administration (FAA) in the United States, and the Joint Aviation Authorities (JAA) in Europe, require that aircraft turbine jet engines safely contain fan, compressor and turbine blades should they be ejected during operation [1]. To achieve this requirement all commercial turbine jet engines include some type of engine blade containment system. In some cases this consists of a metal ring that is thick enough and strong enough to prevent penetration of a blade. Steel, aluminum and titanium systems are currently in use. Other systems are more complex, consisting of relatively light metal or composite rings, a structure such as honeycomb to provide stiffness, and a series of layers of woven aramid fabric to contain the blade. Fabric systems can substantially reduce the weight [2]. However, for high temperature applications, such as around parts of the compressor and the turbine region, or in supersonic applications where conditions are more demanding, it is necessary to use metal containment systems.

While metal systems can be heavy, it is possible to minimize the weight through proper design, material selection and material heat treatment. However, other than by conducting ballistic impact tests, there is currently no reliable method to predict how a material will perform under impact conditions. Sophisticated computer programs are available to simulate impact events, but they rely on accurately modeling the constitutive behavior and deformation and fracture mechanisms that occur. This is still an area of active research and is not yet at a point where accurate predictions of material behavior can be obtained.

There have been a number of investigations aimed at correlating ballistic impact performance with relatively easily measured material properties. A review of some of these studies [3] indicated that hardness measurements of steel armor showed surprisingly good correlation with ballistic penetration properties, and that there was also some correlation between Charpy impact test values and the ballistic limit, the velocity required for a projectile to penetrate a specimen in a particular test configuration. A study by Sangoy et al. [4] concluded that a basic requirement for ballistic armor is that it have high hardness. An interesting conclusion of this study was that for low hardness steels, where failure occurs as a result of plastic flow in the target, and for high hardness steels, where projectile fracture occurs, there is a strong correlation between the target

material hardness and the ballistic limit. However, in the intermediate regime, where the failure is dominated by adiabatic shear, the ballistic limit decreases with hardness.

Impact tests on two titanium alloys [5] found no correlation between the ballistic limit and either fracture toughness or Charpy V-notch toughness. This was supported by a study by Burkins and Love [6] in which the effects of the annealing temperature on the ballistic limit of Ti-6Al-4V were measured. The results of this study showed that changes in annealing temperature affected the tensile strength, yield strength, strain to failure, toughness and Charpy impact strength. However, there was no clear correlation between any of these properties and the ballistic limit. It should be pointed out that the change in static properties due to the annealing was modest.

Because of its importance in military applications, most of the work cited in the above references, and much of the ballistic impact work in the literature, is relevant to ordnance impact speeds in the vicinity of 1000 m/sec or higher. There appears to be no static property that correlates well with ballistic impact strength, with the possible exception of hardness. At impact velocities that occur in fan containment applications, which are typically less than 500 m/sec, the failure mechanisms are likely to be different from those occurring in high velocity impacts, and the relationship between static material properties and ballistic impact properties could also be different. Empirically based procedures used for containment design currently rate materials according to an approximation of the area under the static stress-strain curve [7]. Since it is unclear what static properties, if any, are correlated with the ballistic limit, and since a good understanding of the failure process is needed to model ballistic failure in containment systems, this study was undertaken. Herein, the failure mechanisms and the relationships between static and ballistic impact properties in Inconel 718, at impact velocities pertinent to jet engine blade containment applications, were investigated.

Materials

Three lots of rolled plate material were used in this investigation. Each lot had a unique thickness (1.0, 1.8, 2.0 mm), so that thickness effects could be studied. The material was purchased to meet AMS Specification 5596 and the composition of each lot, as given by the manufacturer, is shown in Table I. No major compositional differences were observed among the lots.

Heat Treatments.—To investigate how mechanical properties affect ballistic properties, it was desirable to vary the mechanical properties as much as possible. It has been shown that annealed versus aged In-718 yield vastly differing mechanical properties [8]. A small heat treatment study was performed on the 1.8 mm thick material to verify this range of properties. Several rectangular, flat tensile specimens, 150 mm in length by 12.7 mm wide were heat treated to one of several heat treatments shown in Table II.

Static tests were conducted on the specimens at room temperature in a servohydraulic test machine. They were first run in strain control at a strain rate of 0.001/sec. The specimens were loaded up to a strain of 1.9 percent, and then unloaded to zero load. Strain was measured using a 12.7 mm gage length extensometer. These strain measurements allowed an accurate determination of the elastic modulus and the yield points. A diametral extensometer was also used to measure the transverse strain to enable calculations of Poisson's ratio. After the unload, the extensometers were removed and the specimen was loaded to failure in stroke control. A loading rate of 0.076 mm/sec was used.

The tensile curves are shown in Fig. 1. The data fell into two categories; moderate strength and high strain to failure (annealed), and high strength with moderate ductility (aged). Based on the results of these tensile tests, the three conditions A, B and C, shown in Table III, were chosen for use with the ballistic impact tests. In addition, impact test results were compared with those from a previous study [9] on the same material. In the study of [9] the material was treated as shown by condition D in Table III.

The tensile properties for the first three of these heat treatments are given in Table IV. Note that the 0.2 percent yield strength (YS) of the aged material is approximately three times that of the annealed, the ultimate tensile strength (UTS) of the aged is twice that of the annealed, while the ductility of the annealed material is substantially greater than the aged material. Note also the large difference in hardness values; the annealed material is softer. These differences in properties are sufficiently large to allow us to assess any possible effects of tensile properties on ballistic impact behavior. In fact, it would be difficult to find a material which exhibited such a wide range of tensile properties without completely embrittling the alloy and rendering it unsuitable for engineering purposes.

The microstructure of the In-718 plates consisted of equiaxed grains (Fig. 2) with occasional carbide particles. The average grain sizes were an ASTM 6 for the 1.0 mm, ASTM 4 for

the 1.8 mm, and ASTM 9 for the 2.0 mm thick materials. The annealed and aged materials of the same thickness had identical grain sizes.

Ballistic Impact Testing

Ballistic impact tests were conducted on specimens of all three thicknesses shown in Table I. The 1.0 and 1.8 mm impact specimens were treated according to the three conditions shown in Table III. The 2.0 mm impact specimens were only tested in the mill annealed condition (Condition B). The impact specimens were 17.8 cm (7 in.) square panels and were centered and clamped over a 15.24 cm (6 in.) square hole in a 1.27 cm (0.5 in.) thick steel plate. Typical impact specimens are shown in Fig. 3. Specimens used in [9] were 35.5 cm (14 in.) square panels, centered and clamped over a 30.5 cm (12 in.) square hole in a 1.27 cm (0.5 in.) thick steel plate.

The projectile used in the present study and in [9] was a Ti-6-4 cylinder with a length of 2.54 cm (1 in.) and a diameter of 1.27 cm (0.5 in.). The impacting face was flat with a radius of 0.8 mm (1/32 in.) machined around the perimeter of the impacting surface. The hardness of the projectile was 32 HRC and its mass was in the range of 14.05 to 14.20 gm. The projectiles were accelerated toward the specimens at normal incidence using a gas gun with a 1.8 m (6 ft) long, 1.27 cm (0.5 in.) inner diameter barrel shown in Fig. 4. The ballistic limit for each heat treating condition and thickness was determined by conducting a number of impact tests, typically seven, which bracketed as closely as possible the velocity required to penetrate the specimen. The ballistic limit was chosen, somewhat arbitrarily, to be approximately the average of the highest velocity for which no penetration occurred, and the lowest velocity at which penetration occurred. It is estimated that the error in the ballistic limit is within ±6 m/sec (~3%).

A measure of the extent of the impact damage was made by placing the panel on a surface plate and measuring the height of the permanent deformation in the damage zone. The height of the permanent deformation was either the height of the edge of the hole, if penetration occurred, or the maximum height of the dent if penetration did not occur. This measurement will henceforth be called deflection. Some of the specimens were sectioned and mounted for metallographic examination. In addition, microhardness measurements were made in the large deformation areas of the specimens. Standard polishing techniques were used for the In-718. However, due to the intense nature of the deformation, a special etching procedure was devel-

oped to reveal the deformation without burning the surface. The following etching procedure was used: Electrolytically etch at 4V in a solution of 10 g CrO_3 + 100 ml water. Remove stains by swabbing with Tucker's reagent. Repeat as needed.

Results

For the initial heat treatment study, the stress-strain curves fell into two groups (Fig. 1). The annealed material exhibited moderate strength and high elongation while the annealed plus aged material exhibited high strength and moderate elongation. The hardness for these materials was measured to be ~90 HRB for the soft, annealed materials and 45 HRC for the harder, aged materials (C and D). The figure includes the three conditions used in the subsequent impact tests, as well as the heat treatment condition used in [9]. It should be noted that the curve in Fig. 1 designated by "(2) + (4)" was taken from tests on the material from the present study heat treated in the same way as in [9]. However, it is expected that the material with condition D used in [9] would have a similar response to this.

Table V lists the velocities and results of the impact tests, as well as a measure of the resulting deflection that occurred. Impact test velocities for each of the thickness and heat treatment conditions is shown in Figs. 5 to 7. The ballistic limit for each condition extracted from these data is shown in Table VI, and includes the ballistic limit for heat treatment D, taken from [9]. In this table, areal weight refers to the weight per unit area of the material, or simply the product of the density and the thickness. This is a relevant measure for fan containment systems since, in general, the overall geometry of the system will be similar, irrespective of the material used. A plot of these data is shown in Fig. 8 and includes the penetration velocity for the 2 mm thick plate in the mill annealed condition (B). For all thicknesses, the annealed material with a lower hardness, moderate strength and higher elongation had superior impact energy absorbing properties compared to the aged material with a higher hardness, higher strength and moderate elongation. For the 1.0 mm thick specimens there was an average increase of 33 percent in the ballistic impact energy of the annealed over the aged material. For the 1.8 mm thick material the average increase was 25 percent. This is contradictory to results in the literature for high velocity impacts [3,4] where it was found that high hardness materials exhibited greater impact resistance.

Metallographic examination of the specimens showed that for both sets of heat treating conditions, the impact produced a circular band of shear deformation extending from the corners of the projectile at the impacted surface to the back surface of the plate at an angle of roughly 45° from the plate normal (Fig. 9). There was significantly more overall deformation in the annealed specimens than the aged specimens as shown by the amount of deflection in Fig. 10. There was essentially no permanent deformation in the projectiles. Microscopic examination (Fig. 11(a)) showed that the annealed specimen exhibited what appeared to be an intense deformation band originating from the corner of the projectile impact. This band was somewhat ill-defined in structure and extended in width over ~10 grains. In nonperforated samples, the band did not reach the back face of the plate. A higher magnification of this band (Fig. 11(b)) shows that this was not a true band, but rather a collection of intensely deformed grains, which etched darker than the surrounding grains. The surrounding grains were also heavily deformed, but not to the extent of those in the band. A microhardness profile was taken across the band. Vicker's hardness ranged from ~260 (100 HRB) in areas far removed from the band (yet still in the deformed region) to a hardness of ~400 (41 HRC) in the band itself.

The aged samples had a much finer deformation structure as shown in Fig. 12. Attempts to bring out visible shear bands were limited. This was partially due to the multitude of fine slip bands in each grain and partially due to the poor etching characteristics of the aged samples. At areas of intense shear (i.e., projectile impact corners), some evidence of well-defined macroscopic bands was observed, but these were generally short and narrow, often connecting carbide particles. Compared to the apparent bands observed in the annealed material (Fig. 11), the bands in the aged material were much narrower, and often multiple bands could be observed in one grain. Similar microhardness profiles were performed with similar results to those in the annealed material. However, the hardness values were higher in all locations due to the fact that the material was originally aged. The hardness ranged from 400 (41 HRC) remote from the shear zone to 500 (49 HRC) in the shear zone.

Close examination of the back surface of both the aged and annealed materials revealed shear bands at 45° angles to the surface of the plate and at multiple locations near the plug. Shear bands caused a V-notch at the surface of the plate (Fig. 12). In specimens that were not perforated, cracks were observed emanating from the notches and propagating along the shear bands.

These were the only evidence of cracking in the nonperforated specimens. Similar notches and shear bands have been observed in explosively bonded In-718 [10].

Discussion

The results show that annealed In-718 has superior impact resistance to the aged material. The annealed material can absorb more plastic deformation before penetration occurs. This is evident from the deflection measurements in Table V and shown visually in Fig. 10. The static toughness, as measured by the area under the stress-strain curve, is greater for the annealed material than the aged, as shown in Fig. 1. The improvement in impact resistance of the annealed material is consistent with general guidelines for designing containment systems that correlate larger areas under the static stress-strain curve with enhanced impact properties [7]. This measurement of toughness is different from a Charpy or KIC fracture toughness, both of which deal with the energy required to propagate a crack. The area under the stress-strain curve is more related to the absorption of plastic deformation before failure and may not even involve a crack until the last moments of the tensile test. It should be pointed out that for In-718, Charpy impact results also showed that that the annealed material is tougher than the aged [8]. Thus for In-718, Charpy values correlate with ballistic toughness. However, this does not appear to be the case for all materials, as illustrated by the results of Burkins and Love [6] who found no correlation between Charpy impact results and ballistic impact resistance in Ti-6-4.

The hardness of the Ti-6-4 projectile used in the impact tests was intermediate between that of the annealed and the aged target material. In general the ballistic limit velocity decreases when the projectile hardness exceeds that of the target [11]. Therefore it is possible that these test results underestimate the greater effectiveness of the annealed over the aged material. However, the results are relevant to jet engine containment systems in which the fans are typically Ti-6-4.

The annealed material appears to better absorb energy by diffusing the macroscopic shear zone over a wider area (Fig. 11). Whereas Fig. 11 indicates that a diffuse macroshear band is formed, high magnification examination of this area revealed that bands per se are not formed. Instead, the grains in this area of intense shear are just more heavily deformed and therefore etch darker than the surrounding grains. This is also indicated by the microhardness profiles, which revealed a higher hardness in the "band" region, typical of more work hardening (plastic

deformation) and agrees with hardness readings taken near shear bands in other materials [12-15]. At least at low magnification, these apparent bands appear similar to those observed in brass 615, [17] and copper [17,18]. In these cases more homogeneous bands formed under isothermal conditions associated with necking during tensile tests. Broad and diffuse bands were also observed in copper under punch-loaded conditions [19].

In contrast, the aged material does show narrow shear bands, thus constricting the later stages of deformation to thin zones, typical of adiabatic shear bands [20]. It has been suggested [12,21] that shear localization increases with decreasing strain hardening and increasing strength, both of which are exhibited by the aged material. This would explain why the aged material has definite shear band formation and the annealed material does not. Additionally, aged In-718 deforms by the shearing of ordered precipitates [22]. During this process, the precipitates are reduced in size within the slip plane, as succesive dislocations approach and shear the precipitates. Consequently, slip within this active plane is easier than on a neighboring inactive slip system. This would encourage shear bands to be narrow. The annealed In-718 does not have ordered precipitates and therefore slip on an existing system can only get more difficult due to dislocation tangles (work hardening). The zone of deformation spreads to neighboring, weaker planes forming a broad diffuse band. For adiabatic shear to occur, the amount of softening due to the local temperature increase must equal the rate of strain hardening [23]. Softening can be assisted by precipitate shearing. Therefore, one would expect the aged In-718 to have more of a tendency to form adiabatic shear bands than the annealed.

Shear localization can also result from the geometry of the specimen and target and the constraints placed on them [21]. It can be seen in Fig. 8 that for the mill-annealed material, the increase in penetration velocity slowed as the thickness of the specimen increased. A possible explanation for this is that the greater bending stiffness of the thicker (2 mm) panel constrained the amount of deformation that could take place. This in fact can be seen by the reduction in the deflection measurements in Table V. Metallography revealed no difference in the deformation structure as these specimens also contained broad, diffuse bands just like the other annealed samples. The thickest material did have smaller grain size (ASTM 9 compared to an ASTM 6 for the intermediate thickness), but this is not believed to have reduced the slope of the curve. It is more likely that the reduction in the slope of the curve was simply experimental variation since the thick material was from a different study and was added here just for completeness.

Examination of additional thicknesses, especially greater than 2.06 mm, would have helped to clarify whether the slope of the curve continues to increase with increasing thickness, or if it levels off as suggested in Fig. 8. However, the existing impact facility was unable to produce the velocities required to penetrate thicker plates.

Post test analysis of the deformation and fracture behavior of the plates suggest the following scenario. Upon impact, the flat-bottomed projectile compresses the material underneath it. Simultaneously, the plate is deflected in the direction of the impact. Bands of intense deformation form at the location of the projectile corners, but for subcritical velocities do not propagate completely through the thickness. On the back side, shear bands form causing notches on the surface (Fig. 13). Cracks often form within these bands probably due to the high tensile stresses on the back surface. Cracking presumably occurs from the front surface as well, but it was never observed in the non-perforated samples. One can assume that if the velocity is high enough to cause cracking on the front surface, the projectile will perforate the plate. Therefore, front side cracking could be used as a critical condition for predicting failure in these tests. Since the cracks on the back surface will also propagate, there is a competition between the front and back side cracks. This often led to a chiseled-shaped fracture surface.

Summary

Under the conditions used in this study, the softer, annealed Inconel 718 performed significantly better than the harder aged material. This is in contrast to results in the literature for higher velocity impacts, which indicate that ballistic limit increases with hardness. The results presented here suggest that toughness may be a better predictor of ballistic impact resistance for the type of failure mechanism and impact velocity associated with fan containment events with Inconel 718. The results indicate that high elongation and better strain hardening capabilities reduce the tendency for shear to localize and result in an unstable adiabatic shear failure. This supports empirical containment design methods that relate containment thickness to the static toughness.

References

1. Federal Aviation Regulations Part 33.94. U.S. Federal Aviation Administration.

2. Smith, G.T., Composite Containment Systems for Jet Engine Fan Blades. NASA TM–81675. 1981.

3. Wong, A.K and Connors, M.L., A literature survey on correlation of laboratory tests and the ballistic resistance of rolled homogeneous steel and aluminum armors. Army Materials and Mechanics Research Center, Report no. AMMRC SP 72–10, Sept., 1971.

4. Sangoy, L., Meunier, Y. and Pont, G., Steels for ballistic protection. Israel J. Technology, 24, pp. 319–326, 1988.

5. Fanning, J.C., Terminal Ballistic Performance of TIMETAL 62S. Eighth World Conference on Titanium. The Institute of Materials. Birmingham, U.K., 1995.

6. Burkins, M. and Love, W., Effect of Annealing Temperature on the Ballistic Limit Velocity of Ti-6Al-4V ELI plates. Presented at AeroMat '96, June, 1996, Dayton, OH.

7. Giard, J.R., Air Turbine Starter Turbine Wheel Containment, SAE Paper 841546, Aerospace Congress and Exposition, Long Beach, CA, 1984.

8. Aerospace Structural Metals Handbook, Vol. 4, ed. C.Y. Ho, CINDAS/Purdue University, West Lafayette, In, 1997, Code 4103.

9. HSCT Lightweight Fan Containment Final Progress Report. Report No. 05 P960828100. Pratt and Whitney/General Electric Aircraft. Aug., 1996.

10. Feng, J., R. Vieira, R.J. Thome and R.M. Pelloux, "Localized Shear Bands in Explosively Bonded Alloy 718/Coper/Alloy 718 Laminates", Superalloy 718 - Metallurgy and Applications, ed. E.A. Loria, TMS, 1989, pp. 407–416.

11. Anderson, C.E., Jr., Hohler, V, Walker, J.D. and Stilp, A.J., The influence of projectile hardness on ballistic performance, Int. J. Impact Engineering, 22, 1999.

12. Rogers, H.C. and Shastry, C.V., Material Factors in Adiabatic Shearing in Steels, Shock Waves and High-Strain-Rate Phenomena in Metals, eds., M.A. Meyers and L.E. Murr, Plenum Press, NY, 1981, pp. 285–298.

13. Rogers, H.C. Adiabatic Shearing—General Nature and Material Aspects, Material Behavior Under High Stress and Ultrahigh Loading Rates, eds., J. Mescall and V. Weiss, Plenum Press, NY, 1983, pp. 101–118.

14. Timothy, S.P. and Hutchings, I.M., The Structure of Adiabatic Shear Bands in a Titanium Alloy, Acta Metall., Vol. 33, No. 4, 1985, pp. 667–676.

15. Leech, P.W., Observations of Adiabatic Shear Band Formation in 7039 Aluminum Alloy, Metall. Trans., Vol. 16A, 1985, pp. 1900–1903.

16. French, I.E. and Weinrich, P.F., The Shear Mode of Ductile Fracture in Materials with Few Inclusions, Met. Trans., V7a, 1976, pp. 1841–1845.

17. French, I.E. and Weinrich, P.F., The Influence of Hydrostatic Pressure on the Fracture Mechanisms of Sheet Tensile Specimens of Copper and Brass", Acta Metall., V24, 1976, pp. 317–322.

18. French, I.E. and Weinrich, P.F., The Shear Mode of Ductile Fracture in Commercial Copper, Scripta Met., V11, 1977, pp. 965–968.

19. Winter, R.E., Adiabatic Shear of Titanium and Polymethylmethacrylate, Phil. Mag., V31, 1975, pp. 765–773.

20. Timothy, S.P., The Structure of Adiabatic Shear Bands in Metals: A Critical Review, Acta Metall., V35, No.2, 1987, pp. 301–306.

21. Chou, P.C., J. Hashemi, A. Chou and H.C. Rogers, Experimentation and finite element Simulation of Adiabatic Shear Bands in controlled Penetration Impact, Int. J. Impact Engng., V11, No.3, 1991, pp. 305–321.

22. Sundararaman, M., Mukhopadhyay, P. and Banerjee, S., Deformation Behaviour of γ'-Strengthened INCONEL 718, Acta Metall., Vol. 36, No. 4, 1988, pp. 847–864.

23. Woodward, R.L., Material Failure at High Strain Rates, High Velocity Impact Dynamics, ed. J.A. Zukas, John Wiley and Sons, Inc., 1990, pp. 65–124.

Figure Captions

Figure 1.—Effect of heat treatment on the room temperature tensile behavior of In-718 sheet specimen.

Figure 2.—Microstructure of Inconel 718 after annealing at 1038 °C.

Figure 3.—Typical test specimens in the initial, non-perforated and perforated conditions.

Figure 4.—50 caliber gas gun facility.

Figure 5.—Impact velocity and penetration results for Inconel 718 annealed at 1038 °C-condition A.

Figure 6.—Impact velocity and penetration results for Inconel 718 in the as-received condition-condition B.

Figure 7.—Impact velocity and penetration results for aged Inconel 718-condition C.

Figure 8.—Impact velocity and penetration results for Inconel 718 as a function of areal weight and heat treatment.

Figure 9.—Shear deformation pattern in impacted specimen.

Figure 10.—(a) Comparison of overall deformation in aged specimens. (b) Annealed specimen. Each specimen was impacted at a velocity slightly below its ballistic limit.

Figure 11.—(a) Region of intense shear deformation in annealed specimen. (b) Higher magnification shows a collection of intensely deformed grains rather than highly localized shear bands.

Figure 12.—(a) Region of intense shear deformation in aged specimen. (b) Higher magnification shows a highly localized shear bands.

Figure 13.—Notches on back surface produced by hgih tensile stresses and the resulting shear bands.

Table I.— Composition of In-718 plates (wt. %)

Thickness (mm)	Ni	Fe	Cr	Nb	Mo	Ti	Al	Mn	Si	Ta	Co	C
1.0	52.8	bal.	18.2	5.05	2.98	1.03	0.51	0.22	0.14	<.05	0.11	.05
1.8	52.3	bal.	18.2	5.11	3.04	1.05	0.50	0.22	0.14	<.05	<.05	.05
2.0	52.7	bal.	18.4	5.13	3.06	1.00	0.54	0.10	0.08	.02	.08	.04

Table II.—Heat treatments used for static testing

Annealing conditions
1) Annealed at 1037°C/1h in vacuum + quick cool in argon
2) Annealed at 954°C/1h in vacuum + quick cool in argon
3) Mill-annealed (as-received condition)
Aging conditions
Anneal (1) + 718°C/8h in vacuum, cool at 38°C/h to 621°C, hold at 621°C/8h, quick cool in argon
Anneal (2) + 718°C/8h in vacuum, cool at 38°C/h to 621°C, hold at 621°C/8h, quick cool in argon
Anneal (1) + 760°C/6h in vacuum + quick cool in argon
Anneal (2) + 760°C/6h in vacuum + quick cool in argon

Table III.—Annealing and aging conditions chosen for impact testing

Heat Treatment Designation	Condition
A	Annealed at 1037°C/1h (vac.) + quick cool
B	As received condition (mill-annealed)
C	A + 718°C/8h (vac.), cool at 38°C/h to 621°C, hold at 621°C/8h, quick cool
D[1]	B + 718°C/8h, cool at 38°C/h to 621°C, hold at 621°C/8h, air cool

[1]Heat treatment used with 350×350 panels from Ref. [9].

Table IV.—Mechanical properties of tensile specimens

HT designation	Modulus, E (GPa)	Poisson's ratio	$YS_{0.2\%}$ (MPa)	UTS (MPa)	Failure strain (%)	Reduction in Area (%)	Hardness HRB (HRC)
A	198	0.29	331	821	67	46	84 (-)
B	198	0.28	483	924	55	43	96 (-)
C	205	0.26	1117	1338	20	30	114 (45)

Table V.—Impact Test Results

Spec. ID	Thickness (mm)	Heat Treat Condition	Rockwell Hardness	Deflection Height, h (mm)	Damage Type	Impact Velocity (m/sec)
GA70	1.83	Annealed	95 HRB	18.0	Perforated	281
GA71	1.83	Annealed	95 HRB	18.0	Perforated	275
GA72	1.85	Annealed	95 HRB	17.9	Perforated	273
GA73	1.80	Annealed	95 HRB	20.0	Non	258
GA74	1.85	Annealed	95 HRB	17.8	Perforated	269
GA75	1.80	Aged	45 HRC	10.8	Perforated	258
GA76	1.83	Aged	45 HRC	9.4	Perforated	248
GA77	1.85	Aged	45 HRC	9.9	Non	226
GA78	1.80	Aged	45 HRC	10.9	Non	243
GA79	1.83	Aged	45 HRC	9.2	Perforated	245
GA60	1.04	Annealed	95 HRB	23.6	Non	190
GA61	1.07	Annealed	95 HRB	23.9	Non	192
GA63	1.04	Annealed	95 HRB	23.6	Non	193
GA64	1.12	Annealed	95 HRB	25.0	Non	198
GA62	1.04	Annealed	95 HRB	14.3	Perforated	200
GA65	1.04	Aged	45 HRC	8.4	Perforated	187
GA66	1.07	Aged	45 HRC	10.3	Perforated	175
GA67	1.04	Aged	45 HRC	10.2	Non	167
GA68	1.12	Aged	45 HRC	10.4	Non	172
GA69	1.09	Aged	45 HRC	9.2	Perforated	166
GA87	2.06	Mill Anneal	82 HRB	11.7	Perforated	297
GA88	2.06	Mill Anneal	82 HRB	14.8	Non	262
GA89	2.06	Mill Anneal	82 HRB	16.5	Non	281
GA90	2.03	Mill Anneal	82 HRB	15.5	Perforated	284

Table VI.—Ballistic limit for In 718

Heat Treatment	Areal Weight (kg/m^2)	Ballistic Limit velocity (m/sec)	Ballistic Impact Energy (J)
A	8.35	198	277
A	14.60	265	497
B	8.35	192	260
B	14.60	277	543
B	16.70	282	562
C	8.35	168	198
C	14.60	244	420
D	8.35	171	206
D	14.60	241	409

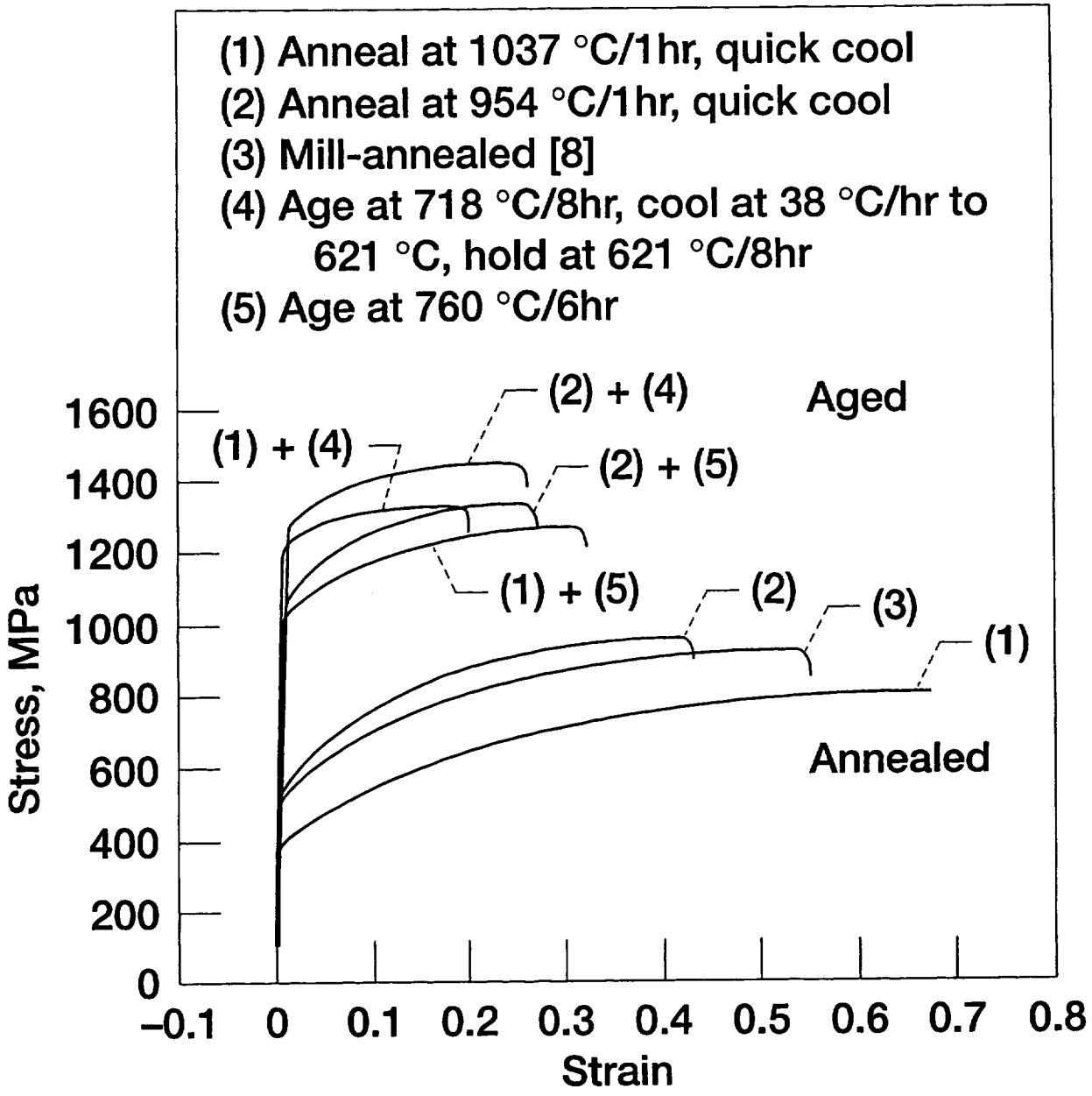

Figure 1.—Effect of heat treatment on the room temperature tensile behavior of In-718 sheet specimen.

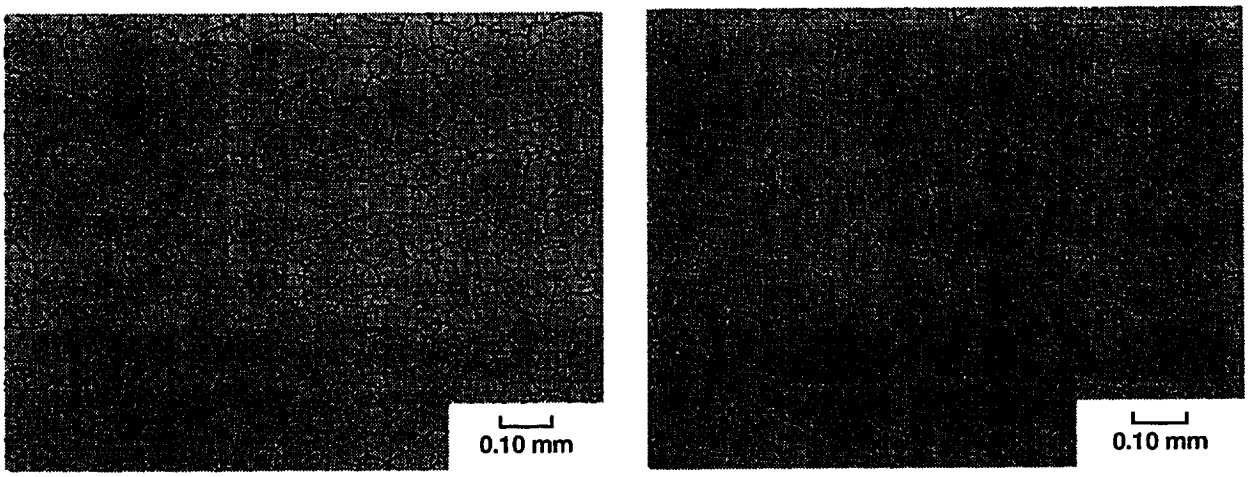

Thickness 1.0 mm

Thickness 1.8 mm

Figure 2.—Microstructure of Inconel 718 after annealing at 1038 °C.

Figure 3.—Typical test specimens in the initial, non-perforated and perforated conditions.

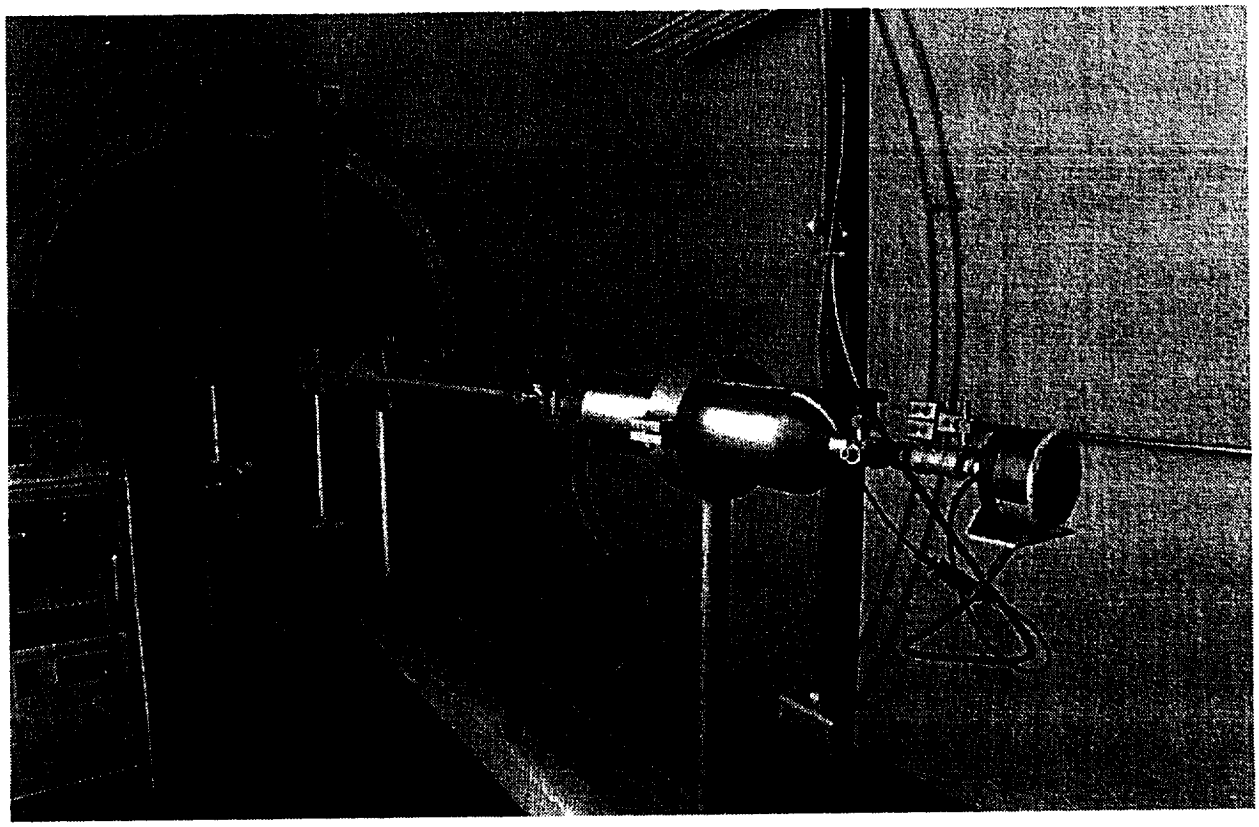

Figure 4.—50 caliber gas gun facility.

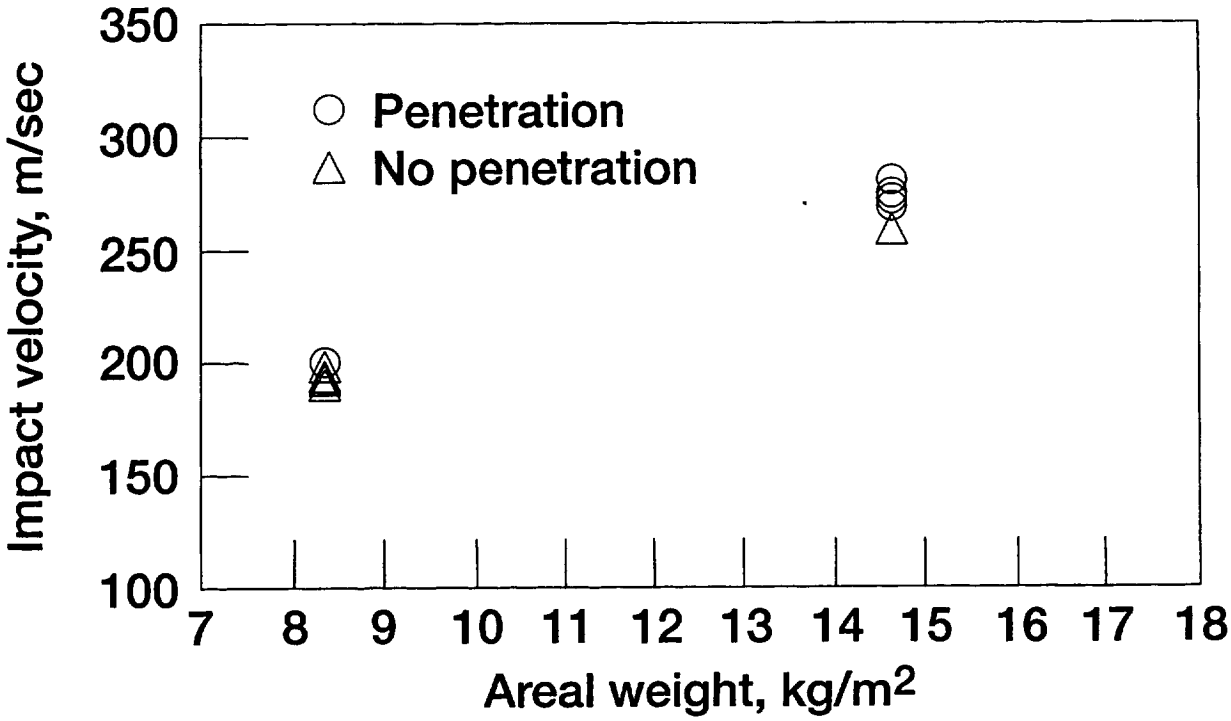

Figure 5.—Impact velocity and penetration results for Inconel 718 annealed at 1038 °C-condition A.

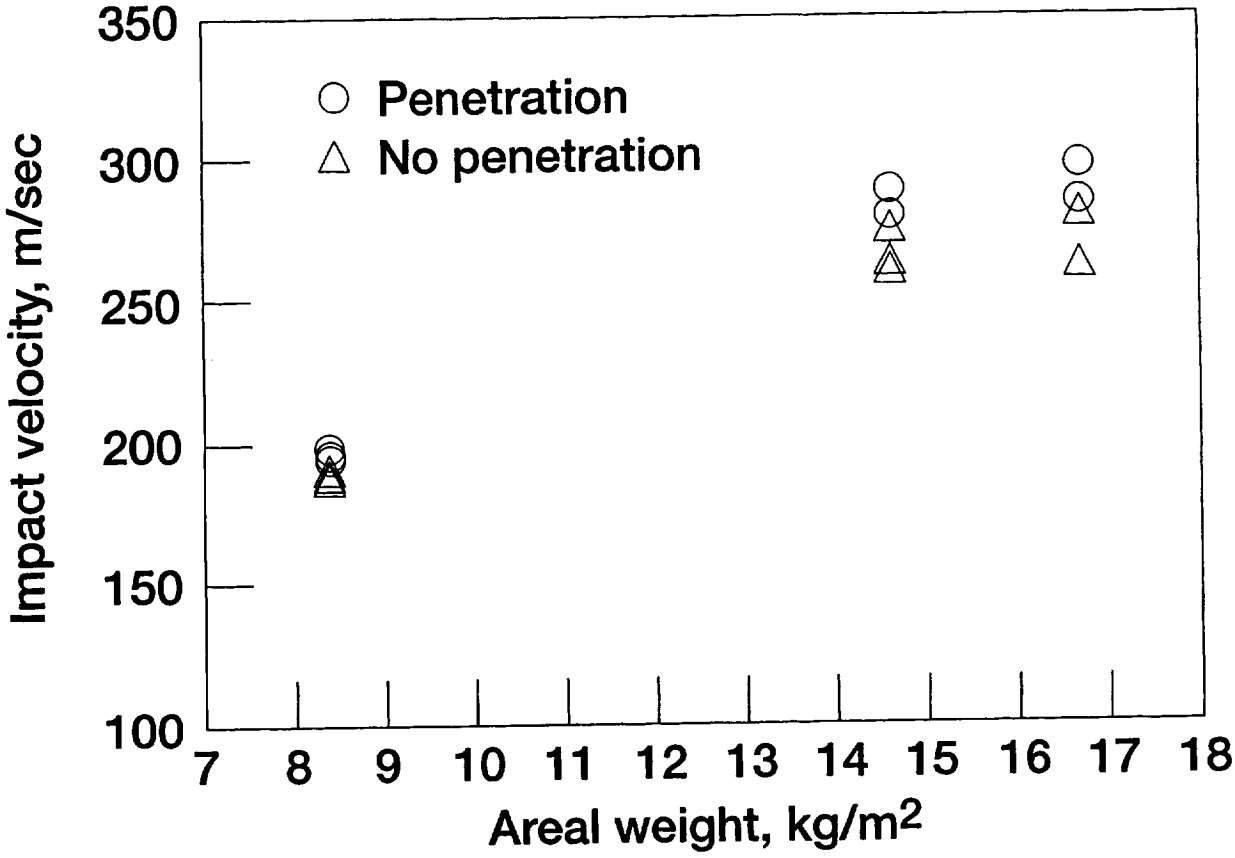

Figure 6.—Impact velocity and penetration results for Inconel 718 in the as-received condition-condition B.

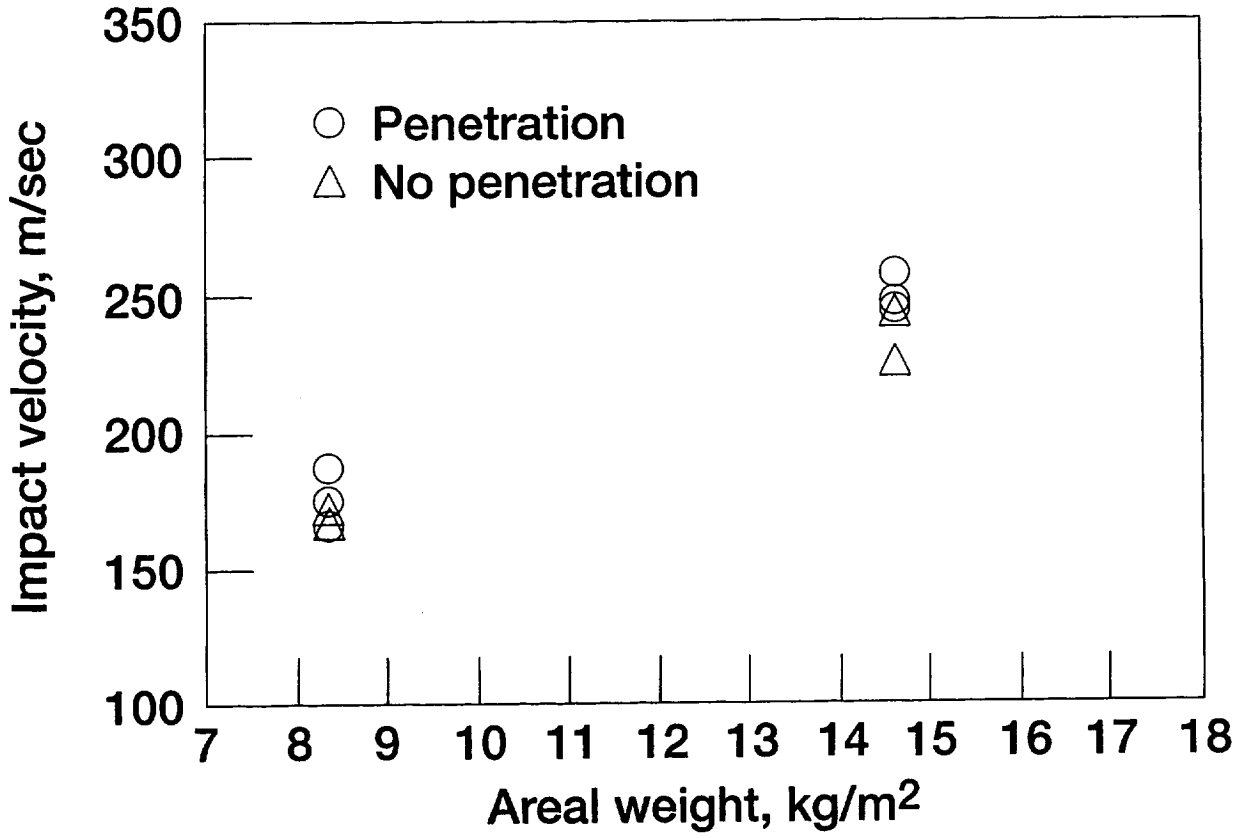

Figure 7.—Impact velocity and penetration results for aged Inconel 718-condition C.

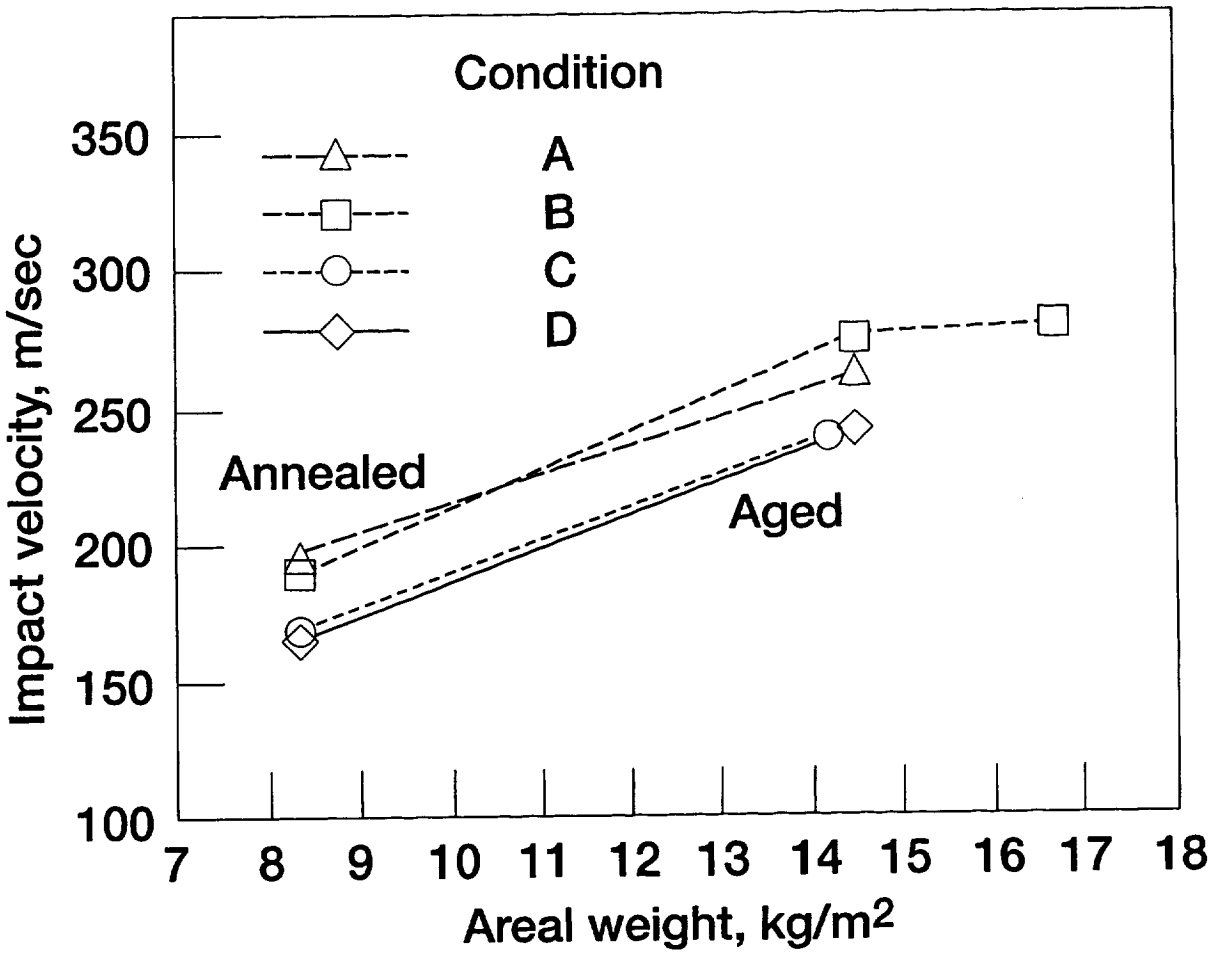

Figure 8.—Impact velocity and penetration results for Inconel 718 as a function of areal weight and heat treatment.

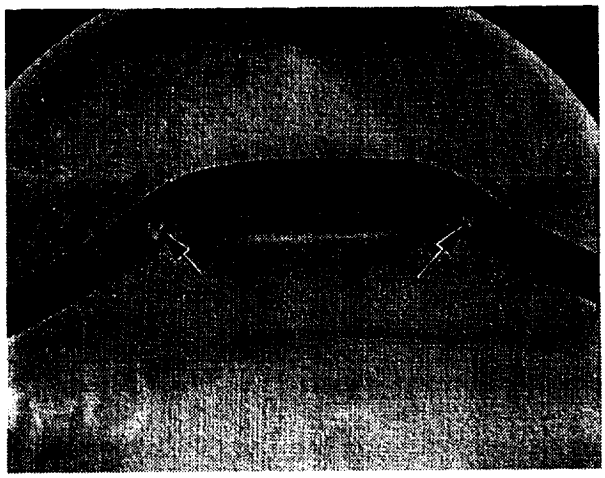

Figure 9.—Shear deformation pattern in impacted specimen.

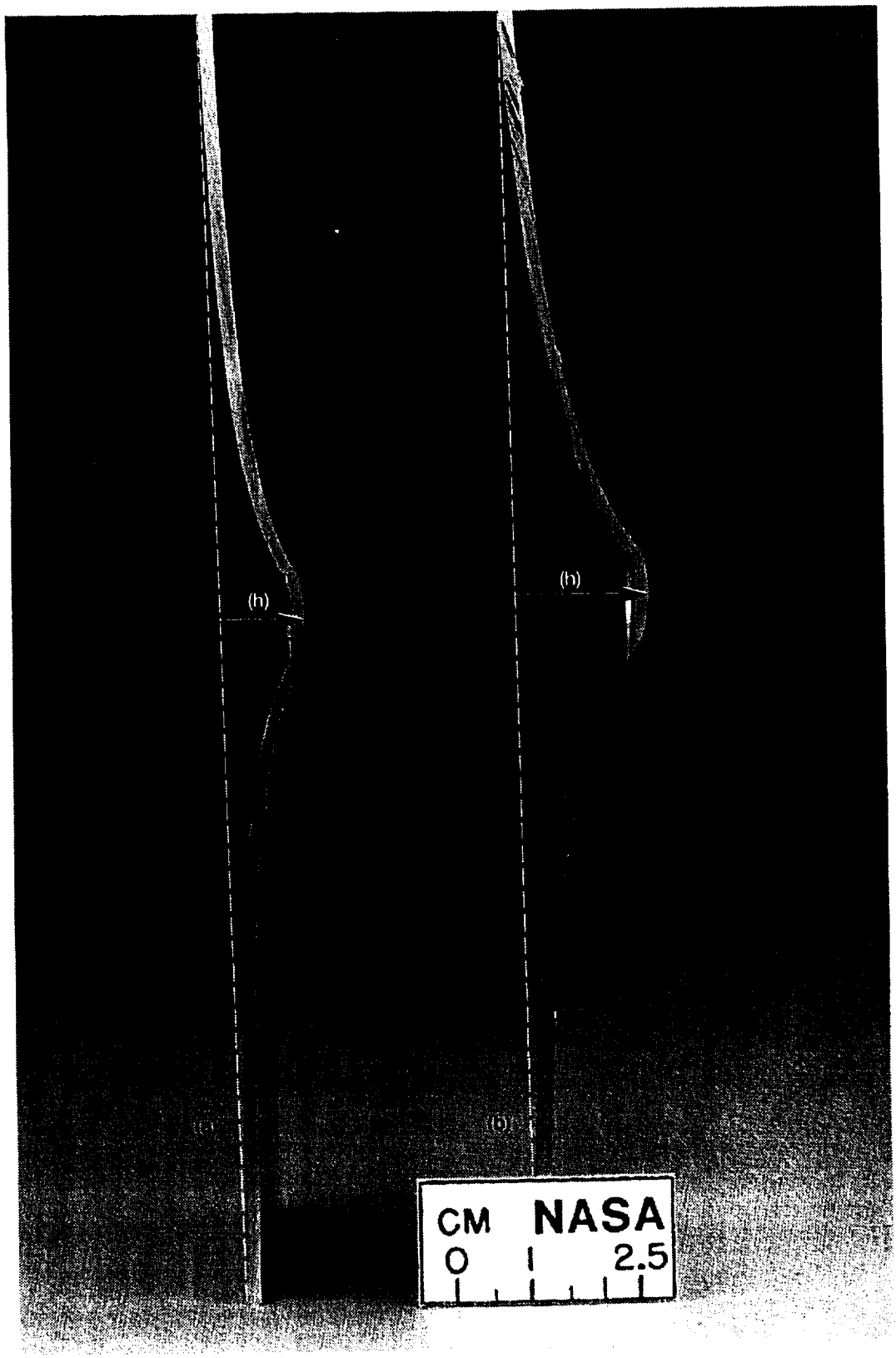

Figure 10.—(a) Comparison of overall deformation in aged specimens. (b) Annealed specimen. Each specimen was impacted at a velocity slightly below its ballistic limit.

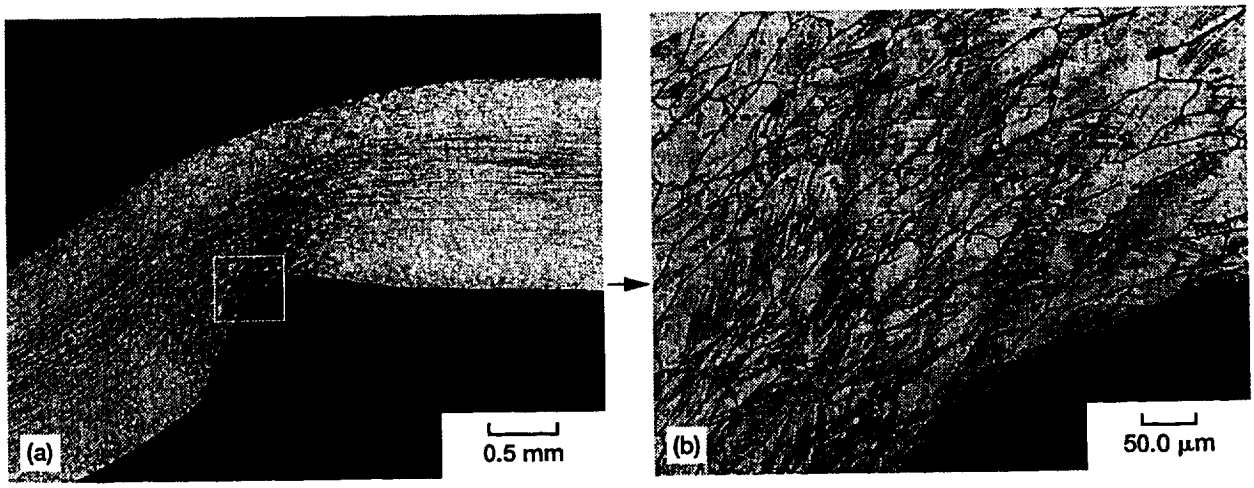

Figure 11.—(a) Region of intense shear deformation in annealed specimen. (b) Higher magnification shows a collection of intensely deformed grains rather than highly localized shear bands.

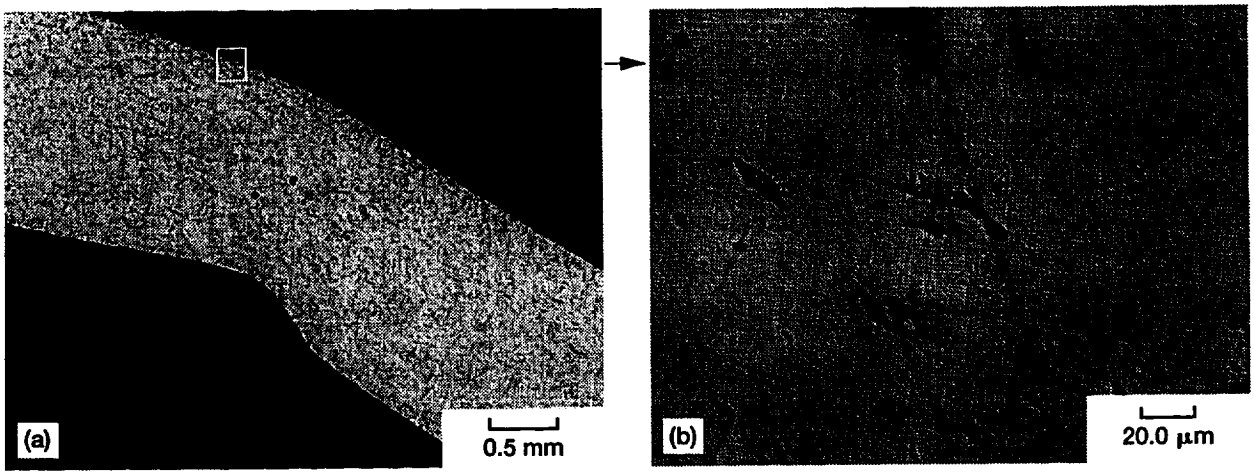

Figure 12.—(a) Region of intense shear deformation in aged specimen. (b) Higher magnification shows a highly localized shear bands.

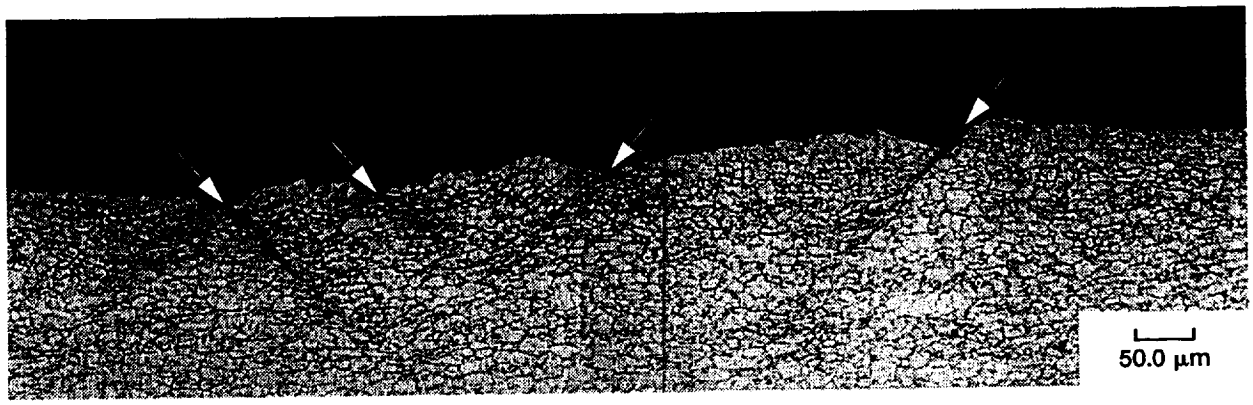

Figure 13.—Notches on back surface produced by high tensile stresses and the resulting shear bands.